ACS APPLIED BIO MATERIALS

www.acsabm.org Article

Poly(allylamine)-tripolyphosphate Ionic Assemblies as Nanocarriers: Friend or Foe?

Eugenia Apuzzo, Maximiliano Agazzi,* Santiago E. Herrera,* Agustín Picco, Gastón Rizzo, Camila Chavero, Daiana Bianchi, Paola Smaldini, María Lorena Cortez, Waldemar A. Marmisollé, Gisel Padula, Analía Seoane, Maria Lis Alomar, Maria Paula Denofrio, Guillermo Docena, and Omar Azzaroni*

Cite This: ACS Appl. Bio Mater. 2023, 6, 4714−4727 Read Online

ACCESS | Metrics & More | Article Recommendations | Supporting Information

ABSTRACT: Designing effective drug nanocarriers that are easy to synthesize, robust, and nontoxic is a significant challenge in nanomedicine. Polyamine-multivalent molecule nanocomplexes are promising drug carriers due to their simple and all-aqueous manufacturing process. However, these systems can present issues of colloidal instability over time and cellular toxicity due to the cationic polymer. In this study, we finely modulate the formation parameters of poly(allylamine-tripolyphosphate) complexes to jointly optimize the robustness and safety. Polyallylamine was ionically assembled with tripolyphosphate anions to form liquid-like nanocomplexes with a size of around 200 nm and a zeta potential of −30 mV. We found that nanocomplexes exhibit tremendous long-term stability (9 months of storage) in colloidal dispersion and that they are suitable as protein-loading agents. Moreover, the formation of nanocomplexes induced by tripolyphosphate anions produces a switch-off in the toxicity of the system by altering the overall charge from positive to negative. In addition, we demonstrate that nanocomplexes can be internalized by bone-marrow-derived macrophage cells. Altogether, these nanocomplexes have attractive and promising properties as delivery nanoplatforms for potential therapies based on the immune system activation.

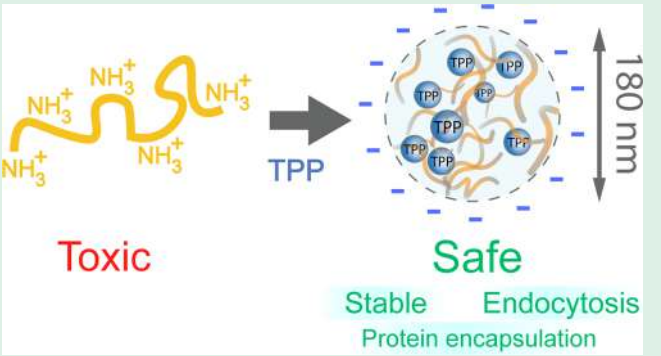

KEYWORDS: *poly(allylamine)-tripolyphosphate nanocomplexes, long-term stability, toxicity switch-off, protein encapsulation, internalization by macrophages*

1. INTRODUCTION

Nanotechnology and materials science are making significant contributions to modern biomedicine by developing a wide range of nanoplatforms with unique properties to improve the delivery of bioactive and therapeutic agents.[1,2] In this scenario, the interaction of nanoplatforms with different cell types, mainly immune system cells such as antigen-presenting cells (APCs), is highly relevant.[3] Among APCs, dendritic cells and macrophages provide the first line of defense against foreign microbes and particulate materials, shaping the adaptive immune response and memory mechanisms. It is well-known that nanoparticulate systems can activate innate immunity through not fully characterized receptors and mechanisms because the activation depends on each nanoparticle and their characteristics such as shape, size, and charge.[4,5] In this way, nanosystems can be used simultaneously to deliver bioactive agents and activate the immune system as adjuvants.[6]

One of the most relevant challenges in nanomedicine is obtaining nanocarriers with simple and sustainable synthetic routes, high drug loading capacity, robustness in physiological environments, and good biocompatibility.[7,8] In this context, nanomaterials based on polyelectrolytes are especially interesting due to the great diversity and availability of this class of polymer.[9,10] In addition, many of these macromolecules are easily solubilized in aqueous media, which allow highly sustainable preparation routes to be applied without the need for the use of toxic and expensive organic solvents. Because of their large number of charges, polyelectrolytes can assemble in an aqueous solution with other oppositely charged species (i.e., polyelectrolytes, surfactants, enzymes, proteins, and multivalent ions) to generate complexes that, depending

Received: July 5, 2023
Revised: October 5, 2023
Accepted: October 10, 2023
Published: October 20, 2023

https://doi.org/10.1021/acsabm.3c00489
ACS Appl. Bio Mater. 2023, 6, 4714−4727

on the experimental conditions, acquire different configurations including complex coacervates, solid precipitates, layer-by-layer films, and nanocomplexes.[11−13]

In recent years, single-polymer aggregates based on polyelectrolytes combined with small molecules bearing multiple charges (multivalent molecules) have attracted great interest in drug delivery applications due to their simplicity of synthesis and ability to load a broad spectrum of bioactive molecules, such as therapeutic drugs, food additives, peptides, and proteins.[10,14] Among them, polyamine-multivalent molecule complexes have been exploited as nanocarriers in different biomedical applications, including tumor treatment, bioimaging, gene therapy, immunotherapy, and infectious diseases.[15] In particular, complexes prepared by mixing of chitosan and sodium tripolyphosphate (TPP) are among the most reported systems.[16] Chitosan has been widely used as a building block due to its bioavailability, biocompatibility, and biodegradability.[17] However, chitosan-based nanocomplexes present relevant disadvantages that make them difficult to use as drug carriers. Chitosan is soluble only in acidic conditions, so it is necessary to produce the complexes in acidic media.[18] Several studies have revealed that chitosan/TPP complexes are unstable at physiological pH (7−7.4) due to the deprotonation of biopolymer amine groups (pK_a ∼6.5) and the consequent destabilization of the complex.[19] In addition, the preparation of these nanosystems presents very poor reproducibility because the polymeric structure can vary significantly depending on the origin of the precursor chitin.[20]

In this scenario, the design of polyamine-multivalent molecule nanocomplexes based on alternative polyelectrolytes can be applied to overcome the limitations of the traditional chitosan/TPP system. Recently, the formation of complexes based on synthetic polyamines such as polyethylenimine and poly(allylamine hydrochloride) (PAH) with oppositely charged small ions has been reported.[21−24] In particular, the complexation of PAH (pK_a ∼8.5) with phosphate-based ions (including TPP) led to the formation of nanocomplexes that remained assembled at physiological pH, independently of the preparation conditions.[25−27] Although these types of systems appear promising, there is still a big gap between the proof of concept and actual clinical use. Furthermore, several studies have shown that synthetic polycations exhibit some form of toxicity toward different cell lines, whereas the manifestation of this toxic behavior is highly dependent not only on the molecular weight but also on the complexation of these cationic polyelectrolytes with different species.[28] For example, the complexation of polycations with negatively charged nucleic acids, which is widely utilized in gene delivery, can reduce the toxicity of the polycations by reducing their overall positive net charge.[29] In addition, polycations have been tailored to decrease their cytotoxicity. The main strategies involved the conjugation of hydrophilic and biocompatible polymers such as poly(ethylene glycol) (PEG),[30] which in addition contributes to minimizing the particle aggregation. In this context, some of the major challenges that need to be addressed include colloidal stability, encapsulation capacities, toxicity, and cell internalization.

In this work, we first studied the physicochemical properties of PAH/TPP complexes by monitoring the experimental parameters where the system acquires a nanosized and short-term stable configuration. Then, the colloidal stability was examined over long storage times and in cell culture media. In addition, the encapsulation capacity was evaluated by using different proteins as model antigens. Cytotoxicity, hemolytic toxicity, and genotoxicity were evaluated under *in vitro* conditions. Finally, the *in vitro* mechanisms of the macrophage cell uptake of nanocomplexes were explored. Taken together, the results show that the PAH/TPP system under certain mixing conditions presents promising properties to act as a powerful, robust, and nontoxic platform for potential applications in protein antigen delivery and active immunotherapy.

2. MATERIALS AND METHODS

2.1. Materials. Sodium tripolyphosphate (TPP), poly(allylamine hydrochloride) (PAH) (Mw ∼17,500), poly(fluorescein isothiocyanate allylamine hydrochloride) (Mw ∼56,000), glucose oxidase from *Aspergillus niger*, bovine serum albumin, cytochrome *c* from equine heart, and lysozyme from chicken egg white were purchased from Sigma-Aldrich. Sodium hydroxide and hydrochloric acid were obtained from Anedra. All chemicals were used without further purification.

2.2. Preparation of PAH/TPP Nanocomplexes. PAH/TPP nanocomplexes were prepared by the direct mixing of components dissolved in water using the following procedure: Two stock solutions of TPP (6 mM) and PAH (10 mM monomer concentration) were prepared using deionized water, and the pH of both solutions was adjusted to 8.5 with 1 M HCl and NaOH. Next, a given volume $V_f/2$ of the PAH solution was placed in a beaker containing a magnetic bar (V_f is the final volume). Then, a volume of $V_f/2$ of the TPP solution was added quickly under constant stirring (1.5 cm long stir bar at 100 rpm) at room temperature. At the moment the TPP is added, the solution goes from translucent to slightly turbid due to the formation of PAH/TPP nanocomplexes. The final concentrations of PAH and TPP in the mixture were 5 and 3 mM, respectively. Although this was the protocol used most in the experiments in this work, different parent concentrations can be used as long as the final concentrations are 5 and 3 mM.

2.3. Preparation of Protein-Loaded PAH/TPP Nanocomplexes. To obtain 2 mL of protein-containing PAH/TPP nanocomplexes, we consecutively mixed the following solutions in a 5 mL beaker under constant stirring (1.5 cm long stir bar at 100 rpm): (1) 250 μL of PAH (40 mM, pH 8.5), (2) 1000 μL of deionized water, (3) 500 μL of protein (1 mg/mL in deionized water), and (4) 250 μL of TPP (24 mM, pH = 8.5). Each solution was added very quickly to avoid heterogeneous reactions, and there was an interval of 5 min between addition steps. The final concentrations of PAH, TPP, and protein in the mixture were 5 mM, 3 mM, and 0.25 mg/mL (25 wt %), respectively. The loading efficiency was evaluated by analyzing the protein content in the supernatant ($C_{protein,\ supernatant}$) after centrifugation of the dispersion at 10,000 rpm (14,000*g*) for 20 min. The bicinchoninic acid method (Thermo Fisher) was used to quantify the protein in the supernatant (all stock protein solutions used for constructing calibration curves were subjected to centrifugation along with protein-loaded nanocomplex samples). The loading efficiency was calculated as

$$\%\text{Loading efficiency} = (0.25\text{mg/mL} - C_{protein,supernatant}) / 0.25\text{mg/mL}) \times 100$$

2.4. Morphological Characterization. PAH/TPP nanocomplex morphology was characterized by transmission electron microscopy (TEM) and atomic force microscopy (AFM). For the TEM measurements, a small drop (∼5 μL) of a PAH/TPP nanocomplex dispersion equilibrated over 1 week was placed in a carbon-coated copper grid and stained with phosphotungstic acid to create image contrast. TEM images were collected with a JEOL microscope (120 kV) equipped with a Gatan US1000 CCD camera. For the AFM measurements, a freshly cleaved highly oriented pyrolytic graphite (HOPG) surface was exposed to a PAH/TPP nanocomplex dispersion for 2 min. Then, the dispersion was gently removed

https://doi.org/10.1021/acsabm.3c00489
ACS Appl. Bio Mater. 2023, 6, 4714−4727

using a N_2 flow. The surface was then analyzed by AFM in tapping mode using a silicon PointProbe Plus Non-Contact Long AFM cantilever (PPP-NCL) with a typical force constant of 48 N/m and a natural frequency of 190 kHz. AFM images were acquired with an Agilent 5500 scanning probe microscope.

2.5. Dynamic Light Scattering (DLS) and ζ-Potential Analysis. DLS and ζ-potential measurements were carried out with a ZetaSizer Nano (ZEN3600, Malvern, U.K.) at 20 and 37 °C using DTS0012 and DTS1060 disposable cuvettes, respectively. For PAH/TPP NP hydrodynamic diameter measurements, a 173° backscatter angle configuration with 20 runs (10 s/run) was used for each sample. Each value of hydrodynamic diameter and polydispersity index was obtained as the average of five consecutive measurements. Nanocomplex ζ-potential was determined from the electrophoretic mobility by laser Doppler velocimetry using a general-purpose analysis method with 100 runs for each sample. To test the stability in physiological-like environments, 300 μL of a dispersion of PAH/TPP nanocomplexes was added to 1 mL of RPMI cell culture medium (Roswell Park Memorial Institute 1640 Medium, Thermofisher) and analyzed by DLS at 25 and 37 °C throughout 24 h.

2.6. Cell Culture. The human lung epithelial cell line A549 was obtained from the American Type Culture Collection (Manassas, VA, USA) and cultured in DMEM (Gibco BRL, Grand Island, NY, USA) supplemented with 10% fetal bovine serum (FBS) from Notocor Laboratories (Cordoba, Argentina) and 50 IU of penicillin and 50 μg/mL of streptomycin from Bagó Laboratories (Buenos Aires, Argentina). The cells were cultured in Falcon T-25 flasks (Nunc, Denmark) under a humidified atmosphere containing 5% CO_2. The A549 cell line was tested for mycoplasma contamination and was found to be free of the bacterium.

2.7. Cell Viability Assays. The cytotoxicity of PAH/TPP nanocomplexes on A549 cells was evaluated by means of the MTT assay. A549 cells were seeded in 96-well plates (Biofil, TCP011096) and allowed to grow for 24 h. After this period, the medium was removed, and the cells were incubated with different concentrations of PAH/TPP nanocomplexes diluted in DMEM supplemented with 10% v/v FBS for 24 h. Dilutions of PAH/TPP nanocomplexes in DMEM were prepared from the PAH/TPP aqueous solutions and cell culture medium, both at 2× (where 1× is the final concentration during incubation). After incubation with PAH/TPP nanocomplexes, the medium was removed, and the cells were washed with phosphate buffer saline (PBS). Next, the cells were treated with a 0.5 mg/mL MTT (3-[4,5-dimethylthiazol-2-yl]-2,5-diphenyltetrazolium bromide) solution for 2 h. In the following, the supernatants were removed, and DMSO was added to solubilize formazan crystals. Finally, the optical density (OD) at 570 nm (using 700 nm as a reference wavelength) was read using a plate reader (Synergy H1 Hybrid Reader, Biotek). As controls of 100% (positive control, PC) and 0% (negative control, NC) cell viability, cells without exposure to PAH/TPP nanocomplexes and cell culture media were used, respectively. The experiments were run in quadruplicates. Cell viability was calculated as %. Cell viability = $[(OD_{sample} - OD_{NC})/(OD_{PC} - OD_{NC})] \times 100$.

2.8. Evaluation of Genotoxicity. Testing for genotoxicity induced by PAH/TPP nanocomplexes on A549 cells was carried out through the use of the comet assay (single cell gel electrophoresis assay) and the micronucleus assay (cytokinesis-block micronucleus cytometry assay).[31] Cells were cultured in monolayers for 24 h and then treated (as explained for the cell viability assay) for another 24 h with selected concentrations of PAH/TPP nanocomplexes for the comet assay. For the micronucleus assay, cells were cultured for another 24 h in the presence of cytochalasin B. All the assays were performed in triplicate to allow an accurate estimate of the interexperimental variation. Bleomycin (1 μg/mL) was used as a positive control for comet and micronucleus assays, and cells grown in DMEM without any other component were used as a negative control. Bleomycin (Gador Laboratories Nippon Kayaku Co., Japan) was dissolved in distilled water before treatment.

The comet assay was performed using a modified alkaline version of the technique described by Singh et al. (PMID: 7488947).[32] The comet assay is capable of detecting DNA damage caused by a variety of factors including strand breaks, alkali-labile sites, and transient repair sites. The first step in the assay involves covering slides with a thin layer of 0.5% normal agarose (Carlsbad, CA, USA) using 180 μL. Then, a mixture of 75 μL of 0.5% low-melting-point agarose (Carlsbad, CA, USA) and approximately 15,000 cells suspended in 15 μL was layered onto the pretreated slides and covered with coverslips immediately. The slides were stored at 4 °C for 10 min for agarose solidification, and then coverslips were removed. Next, the slides were immersed in a freshly prepared lysis solution and stored overnight at 4 °C. Afterward, the slides were equilibrated in an alkaline solution with a pH of 13 for 20 min. The electrophoresis was performed at 1.25 V/cm for 30 min. Following electrophoresis, the slides were neutralized by washing them three times with Tris buffer (pH 7.5) every 5 min and finally washed in distilled water. SYBR Green I staining solution (1/1000, Molecular Probes, Eugene, OR, USA) was used to stain the slides, and 200 randomly selected comet images were analyzed for each treatment.

Scoring was conducted using a Sony 3 CCD-IRIS Color Video Camera connected to a fluorescent microscope with a 515−560 nm excitation filter at 400× magnification. Cells were categorized based on the length of their tails, which corresponds to the degree of strand breakage.[33] The damage index (DI) was calculated following the method of Collins.[33] Visual scoring using arbitrary units is both simple and rapid, and it shows a high correlation with computer image analysis based on the percentage of DNA in the tail.[33]

The micronucleus assay was carried out with slight modifications according to the method proposed by Fenech.[31] Briefly, cells were suspended in a fresh culture medium containing 3 μg/mL cytochalasin B (Sigma, St. Louis, MO, USA) after 2 days of culture and incubated for 26 h. On day 3, the cells were collected and centrifuged. Pellets were then resuspended in 5 mL of fixative solution 1 (6:5:1 sodium chloride/methanol/acetic acid). Afterward, the cells were washed twice with fresh fixative solution 2 (5:1 methanol/acetic acid) and resuspended in this solution. Then, clean slides were used to drop the cell suspension and stained with 5% Giemsa for 10 min. The following chromosome damage biomarkers were scored: micronuclei (MNi), nucleoplasmic bridges (NPBs), and nuclear buds (NBuds). One thousand binucleated cells (BNs) were analyzed for each experimental point to assess cytostatic effects. The nuclear division index (NDI) was used for this purpose. Five hundred viable cells were analyzed per experimental point to determine the nuclear division index (NDI) using the method described by Fenech,[31] which involved scoring the frequency of cells with one, two, three, or four nuclei. The frequency of necrotic and apoptotic cells was determined by scoring 500 cells to assess cytotoxicity. The scoring criteria used included MNi, NPBs, NBuds, and necrotic and apoptotic cell determinations.

2.9. Hemolytic Activity Assays. Fresh blood was collected from sheep by using EDTA as an anticoagulant. Blood was centrifuged (4 °C, 1000*g*, 15 min) to separate red blood cells (RBCs). RBCs were washed four times with physiological solution by cycles of centrifugation (4 °C, 1000*g*, 15 min) and gentle resuspension. A stock RBC suspension (hematocrit ∼10%) was prepared by adding 9 mL of physiological saline to 1 mL of purified RBCs. This stock solution was used in all of the hemolytic assays. All PAH/TPP samples were dispersed in physiological solution in sterile microtubes at room temperature immediately before RBC incubation. A 0.1 mL RBC stock suspension was added to 0.9 mL of sample solutions and incubated for 60 min at room temperature (22 ± 1 °C) under gentle shaking after homogenization. Final PAH/TPP nanocomplex concentrations were calculated considering the final volume of 1.0 mL. Positive (PC, 100% hemolysis) and negative (NC, 0% hemolysis) controls were prepared by incubating RBC with deionized water and physiological solution, respectively.

After incubation, the tubes were centrifuged at 10,000 rpm for 15 min at 4 °C, and 0.2 mL aliquots of supernatant were transferred to a clean 96-well plate. Absorbance (Abs) of released hemoglobin was measured at 540 nm with a microplate reader (Synergy H1 Hybrid Reader, Biotek). Hemolysis percentages were calculated as %

https://doi.org/10.1021/acsabm.3c00489
ACS Appl. Bio Mater. 2023, 6, 4714−4727

hemolysis = $[(Abs_{sample} - Abs_{NC})/(Abs_{PC} - Abs_{NC})] \times 100$. Experiments were performed in triplicates.

2.10. Cell Uptake. *2.10.1. Generation of Bone-Marrow-Derived Macrophages (BMDMs).* Bone-marrow-derived macrophages (BMDMs) are primary macrophage cells derived from bone marrow cells *in vitro* under the influence of growth factors. In this procedure, bone marrow cells are grown in culture dishes with M-CSF. This macrophage stimulating factor was produced in L929 cells, and it was used in the form of an L929-conditioned medium (LCCM). BMDM cells were obtained from the femur and tibiae of BALB/c mice and were differentiated into BMDMs using a previously described protocol.[34] Briefly, cells were seeded on 24-well plates at 5×10^5 cell/mL (day 0) and maintained in Dulbecco's modified Eagle medium (DMEM) containing 10% FBS, 100 U/mL penicillin, 100 μg/mL streptomycin, and 20% LCCM at 37 °C in a 5% CO_2 atmosphere for 7 days. On day 4 of incubation, the medium was fully replaced.

2.10.2. Cell Line Exposure and Characterization. BMDMs were maintained in DMEM containing 10% FBS, 100U/mL penicillin, and 100 μg/mL streptomycin at 37 °C in a 5% CO_2 atmosphere and plated at 1×10^6 cell/mL in 48 wells. Cells were stimulated with 20−30 μL of PAH/TPP nanocomplexes conjugated with FITC for 4 h. To inhibit endocytosis, the stimulation was performed at 4 °C for 4h. For cell characterization, BMDMs were washed with PBS and stained for 1 h at 4 °C with anti-MHCII (PE) and anti-F4/80 (APC) (eBioscience). Fluorescence acquisition was performed with a FACS Aria cytometer. The data were analyzed with the FlowJo software.

For additional characterization, PAH/TPP-exposed BMDMs were washed with PBS, and lysosomes were stained with LAMP-1 and conjugated with Alexa-Fluor 647 (eBioscience). Nuclei were stained with DAPI, and cells were fixed with 4% PFA. Microscopy observations were performed with a Leica SP5 Confocal Microscope.

3. 3RESULTS AND DISCUSSION

3.1. Preparation and Characterization of Nanocomplexes. When mixing two aqueous solutions of PAH and TPP under charge-matching conditions ($[TPP] \approx [NH_2]/5$) at pH 7, an immediate increase in turbidity takes place, indicating that the system separates into two phases. As time evolves, the turbidity decreases, and a rubbery material deposits at the bottom of the tube. Similarly to what happened when mixing two oppositely charged polyelectrolytes, the mixing of the polyamine and the small polyvalent anion first behaves as a colloidal dispersion of small particulate PAH/TPP complexes, and then it evolves into a macroscopic phase separation.[35] For those interested in a more in-depth analysis of the macroscopic phase characterization, we highly recommend a comprehensive study by Lawrence and Lapitsky in which they examine phase transitions under various experimental conditions and delve into the rheological and adhesive properties of the system.[36] It is widely accepted that the colloidal dispersion that is formed at the beginning of the experiment does not represent a thermodynamically stable state but a kinetically trapped state. Lutkenhaus et al. demonstrated that, by regulating the ionic strength and working under nonstoichiometric conditions, the window of stability of the kinetically trapped state in polyelectrolyte complexes could be extended.[37] In this sense, we explored different experimental conditions (PAH concentration, TPP/NH_2 molar ratio, mixing method, and parent solution pH) to find the most stable dispersion for the particular case of the PAH−TPP couple.

We first examined the effect of the PAH concentration and the molar ratio TPP/NH_2 at pH^0 = 8.5 with no added salts (pH^0 is the parent pH of both PAH and TPP solutions). Figure S1 shows the hydrodynamic diameter and polydispersity index (PDI) for PAH/TPP mixtures at 5, 10, 15, and 20 mM NH_2 with varying TPP/NH_2 molar ratios. Here, the most stable dispersions were obtained for $[NH_2]$ = 5 mM and TPP/NH_2 below 0.1 (excess of positive charges) or above 0.25 (excess of negative charges). For all PAH concentrations, the dispersion was highly unstable close to the charge-matching conditions ($[TPP] \approx [NH_2]/5$ or $[TPP]/[NH_2] \approx 0.2$). At this point, it is worth mentioning that the exact relation for zero charge is not known because it will depend on the protonation degree of both reagents, which becomes different than those determined for the individual components due to the pK_a shifting produced by the interaction between them. However, it is reasonable to consider that PAH is fully ionized and TPP carries five charges per molecule (this is just an assumption because we are not focused on the region of zero charge). Next, for $[NH_2]$ = 5 mM and pH^0 = 8.5, we measured the degree of PAH cross-linking as a function of the TPP content. For this, we used FITC-labeled PAH and prepared a series of nanocomplexes with the TPP/NH_2 molar ratio ranging from 0 to 0.6. Then, we subjected the samples to centrifugation and analyzed the content of PAH in the supernatant by means of a UV−vis calibration curve. Figure S2 shows that there is a linear increase in the PAH content between 0 and 0.1 until it reaches a steady value of ∼95%. This result indicates that almost all PAH chains are taking part in the nanocomplex whenever the TPP/NH_2 is above 0.1.

The parameter that we addressed was the initial pH of both the TPP and PAH solutions prior to mixing (pH^0). For this, we prepared a series of PAH/TPP complexes with $[NH_2]$ = 5 mM and $[TPP]/[NH_2]$ = 0.6 at different pH^0 values and determined the hydrodynamic diameter of the nanocomplexes by DLS. Results indicated that the hydrodynamic diameter did not vary significantly between pH^0 = 7 and 8.5 and was placed at around 150 nm with a polydispersity index (PDI) close to 0.05 (Figure S3a). Simultaneously, we measured the pH of solutions after mixing (Figure S3b) and registered a linear increase between the final pH and the initial pH with a slope of 1.5 and an intercept of −3. This indicates that, within the range of pH under study, the complexation between PAH and TPP produces an uptake of protons from the solution, increasing the ionization degree of PAH within the complex (cooperative ionization).[25,38] The result obtained in this work regarding pH changes upon complexation is in full agreement with previous findings by Lawrence and Lapitsky, who, by constructing phase diagrams in the pH^0-TPP/NH_2 and pH after mixing TPP/NH_2 spaces, demonstrated that whereas for $pH^0 < 7$ the complexation process produces a releasing of protons into the media (likely fueled by the deprotonation of TPP ions), for $pH^0 > 7$, the complexation produces an uptake of protons from the solution (ionization of NH_2 groups in PAH), increasing the overall pH.[36] In the same work, Lapitsky also shows that when TPP/NH_2 is high enough (typically above 0.25), the net surface charge of the complex turns negative and the dispersion becomes less unstable.[14]

The protocol for the preparation of PAH/TPP nanocomplexes involves the mixing of PAH and TPP aqueous solutions; however, the mixing methodology can influence the characteristics of the aggregates produced.[39] In this sense, we found that the most critical step of the process is the rate at which the TPP solution is added to the PAH solution. As mentioned before, when $[TPP]/[NH_2]$ = 0.2, the system tends to aggregate very rapidly because all PAH charges are compensated by TPP anions. Therefore, to get a stable

https://doi.org/10.1021/acsabm.3c00489
ACS Appl. Bio Mater. 2023, 6, 4714−4727

colloidal dispersion, the final molar ratio (i.e., $[TPP]/[NH_2]$ = 0.6) must be reached rapidly, avoiding the system being near $[TPP]/[NH_2]$ = 0.2 during the mixture of components. To study the effect of the TPP addition rate, we prepared five solutions, varying the rate of TPP addition. When the TPP is added drop by drop from a buret, the hydrodynamic diameter increases significantly and the colloidal dispersion is highly unstable (Figure S4a), yielding a highly turbid mixture (Figure S4b). Similar results were obtained when the TPP solution was added in 5 and 10 aliquots. Note that when adding the TPP in 5 or 10 aliquots, a molar ratio of $[TPP]/[NH_2]$ = 0.24 is obtained at the second or fourth aliquot, respectively. When adding the TPP in two aliquots, the system behaved almost identically to the one obtained when adding the TPP solution in one shot. After the first aliquot, a molar ratio of $[TPP]/[NH_2]$ = 0.3 is obtained, which is enough away from the critical point.

Summarizing the results above, we established the experimental conditions (pH, concentrations, and mixing procedure) that maximized the long-term stability of the PAH/TPP system in colloidal dispersion. These conditions are the following: (1) $[NH_2]$ = 5 mM, (2) [TPP] = 3 mM (which corresponds to a molar ratio $[TPP]/[NH_2]$ = 0.6), (3) initial pH of the PAH and TPP solutions adjusted to 8.5, and (4) fast mixing of solutions. After establishing these parameters, we studied the reproducibility of the synthesis and found that the complex formation was highly reproducible, and minimal fluctuations of sizes were detected from batch to batch (Figure S5). Figure 1 shows a schematic representation of the procedure carried out to prepare a stable colloidal dispersion of PAH/TPP nanocomplexes and the process of molecular PAH cross-linking by TPP anions.

The kinetics of nanocomplex growth was monitored by DLS. Immediately after the mixing of components, there is an initial burst of nanocomplex growth from 90 to 120 nm within the first 60 min (Figure 2a) that is coupled with an increase in the pH of the solution from 8.5 to 10.2 (Figure S3b). All changes registered at this stage are consistent with the ionic cross-linking of PAH chains with TPP anions and a tendency of the polymer to acquire extra charge by uptaking protons from the solution. In the second stage, the nanocomplex size reaches a size of ~150 nm with a polydispersity index below 0.1 that slowly increases to ~200 nm over the following months while maintaining the polydispersity index below 0.3 (Figure 2b). Furthermore, even within the initial 40 days, the derived count rate (which correlates with the concentration of droplets in solution) exhibited minimal fluctuations (Figure S6).

Similarly to other PAH/multivalent molecule systems, PAH/TPP nanocomplexes are spherical, as seen in the image obtained by TEM (Figure 2c).[40] Additionally, PAH/TPP nanocomplexes exhibited typical coacervate nanodroplet characteristics, as demonstrated by AFM (Figure S7), where they were seen to deform upon contact with a hydrophobic surface such as highly oriented pyrolytic graphite (HOPG). On the other hand, the surface charge of the nanocomplexes was found to be negative with a ζ-potential of −30 mV.

Lapitsky and co-workers studied the complex formation process and the phase behavior of different polyamine/multivalent molecule systems such as chitosan/TPP, PAH/pyrophosphate, and PAH/TPP.[41−43] Regarding the kinetics of nanocomplex formation, they found that the process follows a two-step dynamics: first, small complexes are formed very

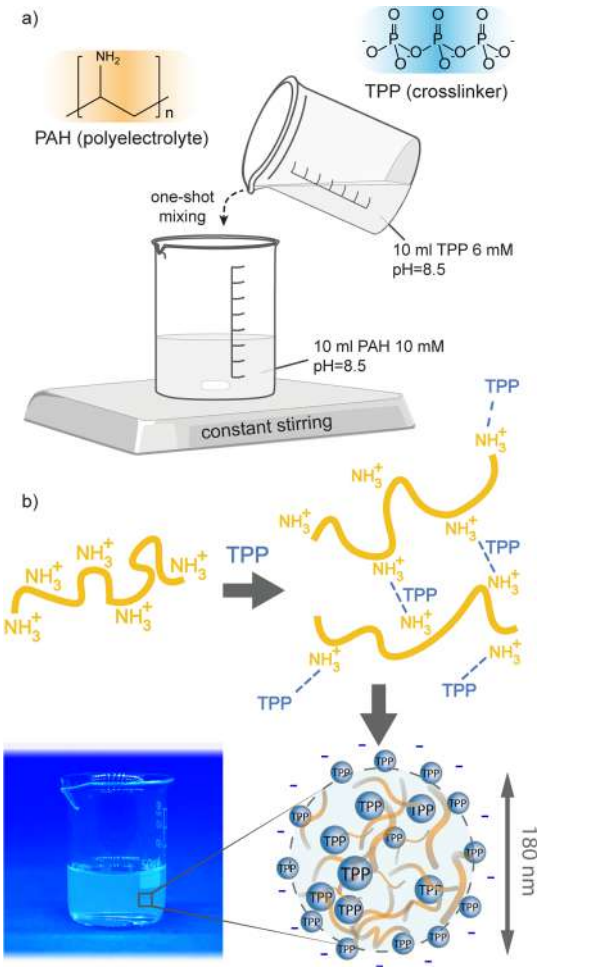

Figure 1. (a) Scheme of the protocol used to prepare a dispersion of PAH/TPP nanocomplexes with enhanced colloidal stability. (b) Simplified representation of the process of PAH cross-linking by excess TPP anions. The photograph corresponds to the solution just after mixing of reagents.

quickly (with only a few polyamine chains), and then they aggregate into larger colloids.[41] As mentioned before, aggregation into a macroscopic phase can be avoided by working in nonstoichiometric conditions. So, why does a molar ratio of $[TPP]/[NH_2]$ = 0.6 give stable colloidal dispersions? PAH is a weak polyelectrolyte with a $pK_{a1/2}$ (value of pH for which half of the amino groups are protonated) of ~8.5.[25] Moreover, the protonation degree of PAH tends to increase when interacting with multivalent anions as in the case of TPP.[25] TPP, on the other hand, is a molecule with five negative charges at alkaline pH and, as PAH, undergoes cooperative ionization in the presence of other oppositely charged macromolecules. This means that $[TPP]/[NH_2]$ = 0.6 (with a parent pH of 8.5) is effectively a mixture with an excess of negative charges (nonstoichiometric conditions), which is coincident with the obtained ζ-potential value. Therefore, the excess of negative charges on PAH/TPP nanocomplexes establishes repulsive electrostatic interactions between pairs of colloids, avoiding (or retarding) the aggregation phenomenon.

3.2. Colloidal Stability. Typically, coacervate droplets (both made of two polyelectrolytes and of one polyelectrolyte and a multivalent salt) tend to grow rapidly in size by ripening or coalescence.[44] This is an intrinsic property of coacervates

https://doi.org/10.1021/acsabm.3c00489
ACS Appl. Bio Mater. 2023, 6, 4714−4727

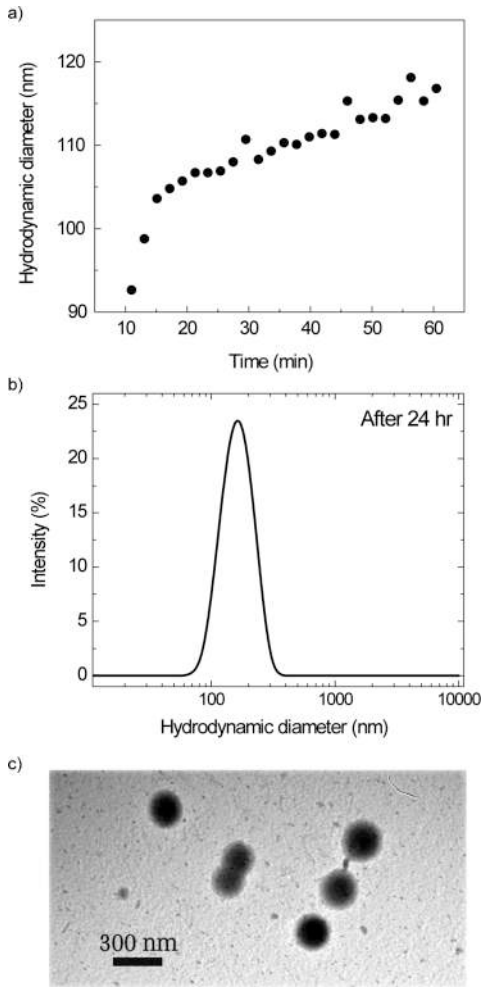

Figure 2. (a) Evolution of the hydrodynamic diameter extracted from DLS measurements during the first 60 min after mixing of reagents for a PAH/TPP solution with $[NH_2]$ = 5 mM, $[TPP]/[NH_2]$ = 0.6, and pH^0=8.5. (b) Distribution of hydrodynamic diameters obtained by DLS for the same solution after 24 h of synthesis. (c) TEM microscopy image of PAH/TPP nanocomplexes obtained under these conditions deposited on a carbon grid.

because colloidal dispersions are not thermodynamically stable phases. For this reason, in general, these systems (including PAH/TPP complexes) have been studied in their microsized and collapsed configurations.[45] Only a limited number of studies have been conducted on nanometer dispersions of the complexes.[35,39] Chitosan/TPP nanocomplexes are among the most reported polyamine/multivalent molecule systems due to the known biocompatibility and bioavailability of chitosan.[46] However, for applications in biomedicine, this system has two major drawbacks that have not been solved yet. First, chitosan/TPP nanocomplexes can undergo disintegration at physiological pH due to the loss of the charge of chitosan.[47] On the other hand, chitosan-based nanocomplexes undergo very fast aggregation in a wide range of conditions, especially in complex matrices, such as cell culture media and blood plasma. Although some authors have reported chitosan nanocomplexes to be stable over month-long experiments in controlled media, it is necessary to extend the storage time even longer for practical applications.[48−50]

Unlike chitosan-based nanocomplexes, PAH-based nanocomplexes have been less exploited. As PAH remains protonated at a physiological pH, the complexation of PAH chains with sufficiently charged small molecules such as TPP leads to the formation of stable nanocomplexes. Moreover, Lapitsky et al. demonstrated that, under certain experimental conditions (i.e., $TPP/NH_2 \gg 0.2$), the PAH/TPP nanocomplex system remains cross-linked within a wide range of pH that goes from pH < 2 to pH ∼ 12.[36,43] Altogether, PAH/TPP nanocomplexes could become an attractive and viable alternative to chitosan/TPP nanocomplexes.

To evaluate the long-term stability of the PAH/TPP nanocomplexes in deionized water, the hydrodynamic diameter and the ζ-potential were monitored over a period of 9 months, with the solution stored in the dark at room temperature without sonication. During the first week, the nanocomplex hydrodynamic diameter increased until reaching a value of 180 nm (Figure 3a). Then, the nanocomplex size remained stable as well as the PDI (0.08 at 9 months) and the ζ-potential values (−25 mV at 9 months) (Figure 3b). Whereas the derived count rate remained relatively stable over 40 days (Figure S6), a significant decrease was observed at 90 days (from 350,000 to 120,000, approximately). This decrease is likely attributed to the adsorption processes of the coacervate droplets onto the surface of the glass container. Through this experiment, we demonstrate that PAH/TPP nanocomplexes are suitable for long-term storage. The months-long stability of the polyamine nanocomplexes can be attributed to their high charge density, which prevents aggregation through electrostatic repulsion. Achieving stable nanocomplexes over an extended period of time is a significant challenge for potential biomedical applications, making this result particularly noteworthy. In most cases, stable core−shell architectures are produced by covalently attaching a water-soluble neutral block to the polyelectrolyte.[51] However, this approach requires synthetic processes that increase the cost and complexity of the carrier preparation process.

In the following, nanocomplexes were subjected to more aggressive conditions to evaluate their stability in physiological-like environments. For this, the PAH/TPP nanocomplexes were dispersed in Roswell Park Memorial Institute 1640 medium (RPMI cell culture medium) and analyzed by DLS at room temperature (25 °C) and 37 °C throughout 24 h. Figure 3c shows that when PAH/TPP nanocomplexes are in contact with RPMI, the hydrodynamic diameter increases up to values between 250 and 300 nm but remains stable without aggregation for both evaluated temperatures. Moreover, the presence of a complex matrix produces an increase in the PDI up to 0.25, denoting an increase in the size heterogeneity (Figure S8). Despite the increase in size and polydispersity, both samples showed a single distribution of nanocomplex hydrodynamic diameters after 24 h of synthesis, as shown in Figure 3d (red and blue lines).

4. PROTEIN LOADING

The encapsulation of proteins is a growing area of interest in biomedical applications, particularly in developing vaccine platforms.[9,52] Although polymeric platforms are increasingly used to encapsulate proteins, traditional manufacturing methods often require organic solvents, which can damage the proteins.[53] To address this issue, polyelectrolyte complexes made using an entirely aqueous process have been proposed as an alternative.[54] Both polyelectrolyte complex coacervates and polyelectrolyte/multivalent molecule complexes have been shown to load proteins within the cross-linked structure.[23,55]

https://doi.org/10.1021/acsabm.3c00489
ACS Appl. Bio Mater. 2023, 6, 4714−4727

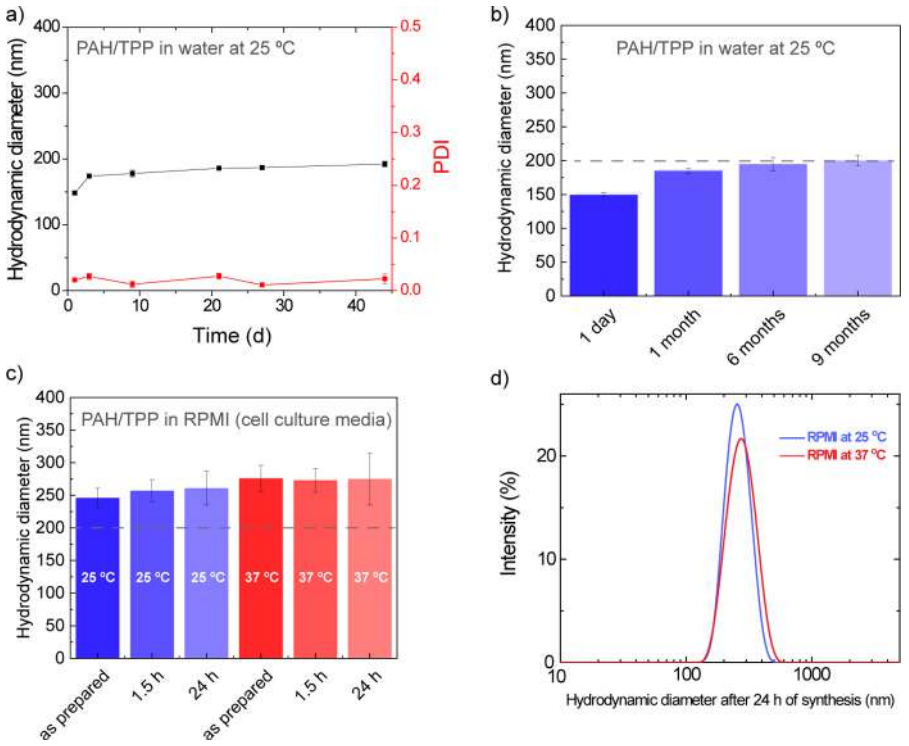

Figure 3. Evolution of the hydrodynamic diameter of PAH/TPP nanocomplexes during (a) the first 40 days and (b) 9 months after synthesis. (c) Hydrodynamic diameter of PAH/TPP nanocomplexes dispersed in Roswell Park Memorial Institute 1640 (RPMI) cell culture media at 25 °C (blue bars) and 37 °C (red bars) at different intervals of time before synthesis. (d) Distribution of nanocomplex sizes for PAH/TPP nanocomplexes dispersed in RPMI at 25 °C (blue line) and 37 °C (red line) after 24 h of synthesis.

The adsorption of proteins is driven by a combination of electrostatics and weak interactions in a similar fashion as PAH chains interact with TPP molecules.[56] In this context, we studied the ability of the PAH/TPP nanocomplexes to load different proteins with different molecular weights and isoelectric points. We tested the loading efficiency for glucose oxidase (160 kDa, pI = 4.2), bovine serum albumin (BSA, 66 kDa, pI = 4.75), cytochrome *c* oxidase (Cyt *c*, 12.4 kDa, pI = 10.25), and lysozyme (14.3 kDa, pI = 11.0) with a final concentration of 0.25 mg/mL (25 wt %). In each case, the protein was first mixed with the PAH solution, and then TPP was added. The plot in Figure 4a shows the loading efficiencies for the different proteins under study, which range from 15 to 20%. According to Perry et al., proteins tend to bind more strongly within complex coacervates only in a narrow window of charge ratios.[55] More specifically, proteins interact strongly with complex coacervates when the fractions of negative and positive charges are close to 0.5 (stoichiometric conditions). In our case, $[TPP]/[NH_2] = 0.6$, which is equivalent to a fraction of negative charges of 0.75. Thus, loading efficiencies of around 15% are not surprising. Interestingly, we observed no tendencies with respect to the isoelectric point. In other words, the loading efficiency is independent of the charge of the protein. This was unexpected because we would guess that proteins will preferentially bind to oppositely charged species (note that the nanocomplex is negatively charged because of the excess of negative charges coming from TPP anions).

We characterized the protein-loaded nanocomplexes by DLS. For this, we first assembled the nanocomplex in the presence of proteins and then waited 24 h to stabilize the system prior to DLS measurements. As depicted in Figure 4b, negatively charged proteins (BSA and GOx) showed almost no

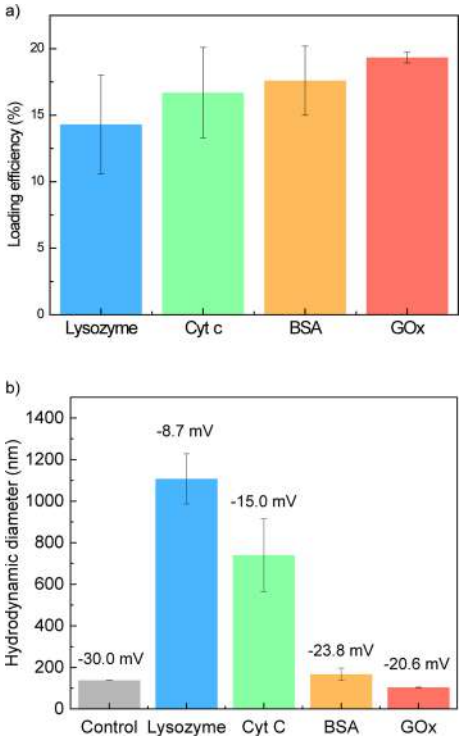

Figure 4. (a) Evaluation of the capacity of PAH/TPP nanocomplexes to encapsulate lysozyme, cytochrome *c* oxidase (Cyt *c*), bovine serum albumin (BSA), and glucose oxidase (Gox). (b) Hydrodynamic diameter of protein-loaded nanocomplexes and their respective ζ-potential values. Error bars correspond to the standard deviation (experiments were performed in triplicate).

https://doi.org/10.1021/acsabm.3c00489
ACS Appl. Bio Mater. 2023, 6, 4714−4727

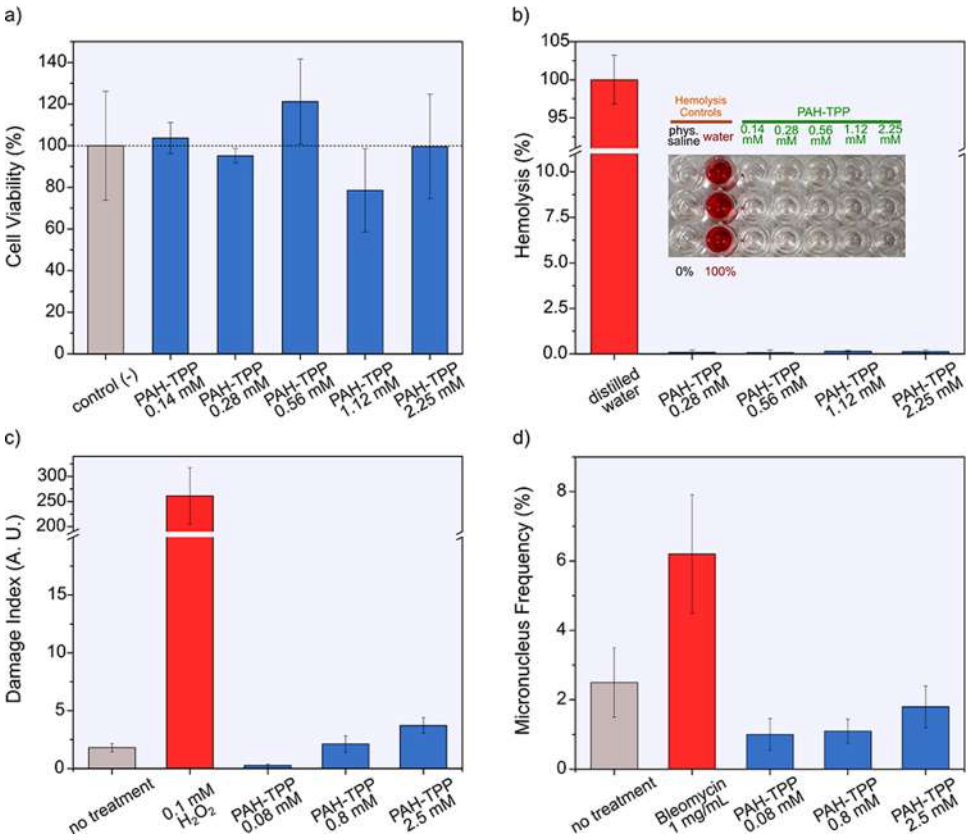

Figure 5. Evaluation of PAH/TPP nanocomplexes toxicity *in vitro*. (a) A549 cell viability with an increasing concentration of PAH/TPP nanocomplexes. Negative control refers to cells incubated with cell culture media only. (b) Hemolytic activity of PAH/TPP tested using sheep RBCs. The inset shows the supernatants obtained after centrifugation of RBCs incubated with PAH/TPP nanocomplexes (in triplicate; prior optical density measurement). (c, d) Results from comet and micronucleus assay performed on A549 cells incubated with PAH/TPP nanocomplexes, respectively. H_2O_2 and bleomycin are positive controls (damage). In all cases, the informed concentrations are based on PAH.

effect on nanocomplex size and surface charge. However, when testing positively charged proteins (lysozyme and cytochrome *c* oxidase), we detected a marked increase in nanocomplex hydrodynamic diameters. Also, the increase in the hydrodynamic diameter was accompanied by a decrease in the ζ-potential. As a possible explanation for these results, we can argue that positively charged proteins (high isoelectric point) do not participate in the complex formation and preferentially bind to the outer sphere of the nanocomplex (protein adsorption), therefore increasing the size and lowering the overall surface charge of the complex. On the other hand, negatively charged proteins (low isoelectric point) do participate in complex formation acting as a second anionic cross-linker and burying inside the complex (protein loading). Notably, we did not detect the formation of macroscopic complexes between PAH and BSA (without TPP) under the same experimental conditions. This result does not necessarily imply that soluble PAH/BSA complexes are not formed.[57]

5. TOXICITY STUDIES

Another important topic in the development of polyamine-containing nanocarriers is their potential toxicity. Polycations like chitosan,[58] polyethylenimine,[59] poly-L-lysine,[60] and PAH,[61] among others, usually present cytotoxic issues frequently attributed to their exposed positive charges and the interaction of these with negatively charged biomolecules (e.g., phospholipids in plasmatic membranes) that can lead to cellular function impairment (e.g., membrane disruption). One approach used to reduce cell toxicity involves screening amino groups by grafting polyamines with PEG.[62] For instance, it has been recently reported that PEGylation of PAH reduces the toxicity of PAH/phosphate nanocomplexes.[63] The authors found that a core−shell structure is formed with the PEG chains forming the outer layer. This PEG shell around a polyamine core shields the positive charges of the PAHs, reducing the zeta potential from +20 mV for unmodified complexes to less than +5 mV for the nanocomplexes based on PAH-PEGylated. Although PEGylation has been shown to be an effective method for reducing toxicity, it may not be ideal for carriers intended for immune system targeting. This is because PEG can create a steric hindrance that limits the penetration of antigen-presenting cells, such as macrophages and dendritic cells, and prevents engulfment of the nanocarrier.[19] Another strategy involves complexation of protonated amines with other ionic structures of opposite charge, which helps decrease these undesirable effects compared with free protonated amines. Sasaki et al. demonstrated that gene delivery nanocarriers composed of ionically complexed polylysine and small interfering RNA (siRNA) induced cellular and hematological toxicity due to their highly cationic character (zeta potential $\sim$ +40 mV).[64] To enhance biocompatibility, γ-polyglutamic acid was added as a third component in the formulation. This biodegradable anionic polymer led to the formation of ternary complexes with an excess of negative charge ($\xi < 0$), which reduced the toxicity of the system.

https://doi.org/10.1021/acsabm.3c00489
ACS Appl. Bio Mater. 2023, 6, 4714−4727

In this study, our aim was to carefully adjust the preparation conditions, particularly the PAH/TPP molar ratio and pH, to successfully produce nanocomplexes that did not induce substantial toxicity. However, it is crucial to note that free polycations can still induce toxic effects even at very low concentrations.[65] Therefore, comprehensive characterization of the toxic profiles of the nanocomplexes is essential. As such, cell viability and hemolytic activity as well as comet and micronucleus assays were performed to evaluate the *in vitro* toxicity of the PAH/TPP nanocomplexes.

The cytotoxicity of PAH/TPP nanocomplexes ($[NH_2]$ = 5 mM, $[TPP]/[NH_2]$ = 0.6, pH^0 = 8.5) was assessed in cell line A549 (human lung carcinoma) by means of an MTT assay.[66] A549 cells are recommended for testing *in vitro* nanocomplex toxicity [ISO 19007:2018]. Results are listed in Figure 5a. Cells exposed only to cell culture media were used as negative control of cytotoxicity (100% of viability). The nanocomplex concentration is expressed as the NH_2 concentration after dilution of the stock PAH/TPP solution. As can be seen, no statistically significant differences in A549 cell viability exposed to PAH/TPP nanocomplexes up to 2.25 mM were observed compared to the negative control ($p > 0.05$). These results are in line with previous findings by Lawrance et al., who demonstrated that PAH/TPP ionically cross-linked polymer networks were essentially noncytotoxic when tested in human dermal fibroblasts.[42] In contrast, the free PAH induced cytotoxicity above ∼1 mM and dramatically reduced cell viability at 2.25 mM (Figure S9). This behavior is attributed to the polycationic nature of PAH.[67]

To evaluate the hemocompatibility and the membranolytic potential of PAH/TPP nanocomplexes, hemolytic activity tests were performed by using sheep red blood cells (RBCs). Considering that sheep RBCs are very fragile compared to RBCs from other mammals,[68] the analysis performed here is supposed to be of high sensitivity for detecting hemolysis induced by the PAH/TPP nanocomplexes. Distilled water, which is hypotonic compared to the RBCs, was used as positive control for 100% of hemolysis, whereas physiological saline, which is isotonic with RBC, was used as 0% hemolysis control.[69] The inset of Figure 5b illustrates the outcomes of centrifugation after the RBCs were incubated with distilled water or physiological saline. The supernatant from RBCs incubated with distilled water exhibited an intense red color due to the released hemoglobin, whereas the supernatant from RBCs incubated with physiological saline showed no color. Regarding PAH/TPP nanocomplexes, no hemolytic activity was detected in the entire concentration range tested (same as used for cell viability assays), as can be seen in Figure 5b. On the other hand, free PAH induced hemagglutination, and the formed RBC aggregates settled down during the experiment (see Figure S10). This phenomenon was already observed for PAH and other polycations.[70,71] As a result, the free PAH seemed to induce little hemolysis (<5%). However, the PAH's membranolytic potential, as evaluated through hemolytic activity, might be underestimated because of hemagglutination.

Evaluation of the genotoxic potential of PAH/TPP nanocomplexes or other polyelectrolyte-based nanostructures is less frequently reported in the literature than assessment of their cytotoxicity. Here, the genotoxicity of PAH/TPP nanocomplexes on A549 cells was studied by means of the comet assay and micronucleus assays.[31,32] Whereas the first of these assays detects primary damage to DNA strands (potentially reversible), the second assesses chromosomal abnormalities like aneuploidy and clastogenicity, which are irreversible (inherited by the daughter cells post mitosis). In line with the previously shown experiments where no cytotoxic or hemolytic effects were detected, PAH/TPP nanocomplexes did not induce any increment in DNA damage or micronucleus frequency when compared to the respective negative controls, as evaluated by comet (Figure 5c) and micronucleus (Figure 5d) assays, respectively. For comparison, PAH (at 2.5 mM) was studied using the comet assay, and it was found that the free polycation can induce moderate DNA primary damage (damage index = 32 ± 2.5).

Previously, the cellular toxicity of other polyamine-multivalent ion nanocomplexes was explored.[59,72] However, it is worth noting that neither of these studies conducted hemo- and genotoxicity tests or assessed long-term colloidal stability, which can make a comprehensive comparison with our system challenging. Huang et al. utilized ionic cross-linking with TPP to mitigate the toxicity associated with PEI as a gene transfection agent.[59] They generated nanocomplexes with sizes ranging from 65 to 147 nm, all of which exhibited a positive zeta potential (from 20 to 7 mV) that diminished with increasing TPP content. This decline in the ζ-potential corresponded to a decrease in cell viability. Gupta and co-workers prepared cross-linked polylysine nanocomplexes by utilizing a mixture of phosphate ions and citrates, aiming for the delivery of an exogenous contrast agent.[72] These complexes exhibited an average diameter of ∼225 nm (PDI ∼ 0.3) and a ζ-potential of +16.2. Cytotoxicity studies were conducted using MTT assays incubating HeLa cells with varying volumes of the nanocomplex formulation. The results indicated that cells incubated with 2 and 5 μL of nanocomplexes maintained over 94% viability. Meanwhile, cells exposed to 10 and 20 μL of PLL NPs remained safe, displaying approximately 89 and 82% cellular viability, respectively. However, a decrease in cellular viability was observed when cells were incubated with 50 μL of nanocomplexes (approximately 60% cellular viability).

On the basis of the results of this work, it is possible to state that PAH/TPP nanocomplexes can be considered as not toxic and safe, at least from an *in vitro* point of view. This contrasts with what was observed for the free cationic PAH that exhibited cytotoxicity, hemotoxicity, and genotoxicity. The absence of toxicity might be attributed, in a general way, to the negative charge of the PAH/TPP nanocomplexes (ζ-potential ∼ −30 mV). It is noteworthy that we were able to decrease the cellular toxicity of polyamine without the need to add a third component or modification chemistry of polymer. More importantly, this toxicity reduction was achieved without compromising the colloidal stability.

6. CELL UPTAKE

The innate immune system serves as the body's first line of defense against foreign intruders, including micro-organisms (such as viruses and nano-organisms) and particulate matter (like uric acid crystals, cholesterol, silica, asbestos, nanoparticles, and cellular debris).[73] The main immune cells in eliminating foreign organisms are cells with phagocytic capacities such as monocytes, macrophages, and dendritic cells.[74] Polyelectrolyte-based hydrogels and nanocomplexes have shown to be excellent candidates for subunit vaccine formulations, possessing the ability to load antigens and act as adjuvant agents to activate the immune system.[9] In this framework, understanding how antigen-presenting cells inter-

https://doi.org/10.1021/acsabm.3c00489
ACS Appl. Bio Mater. 2023, 6, 4714−4727

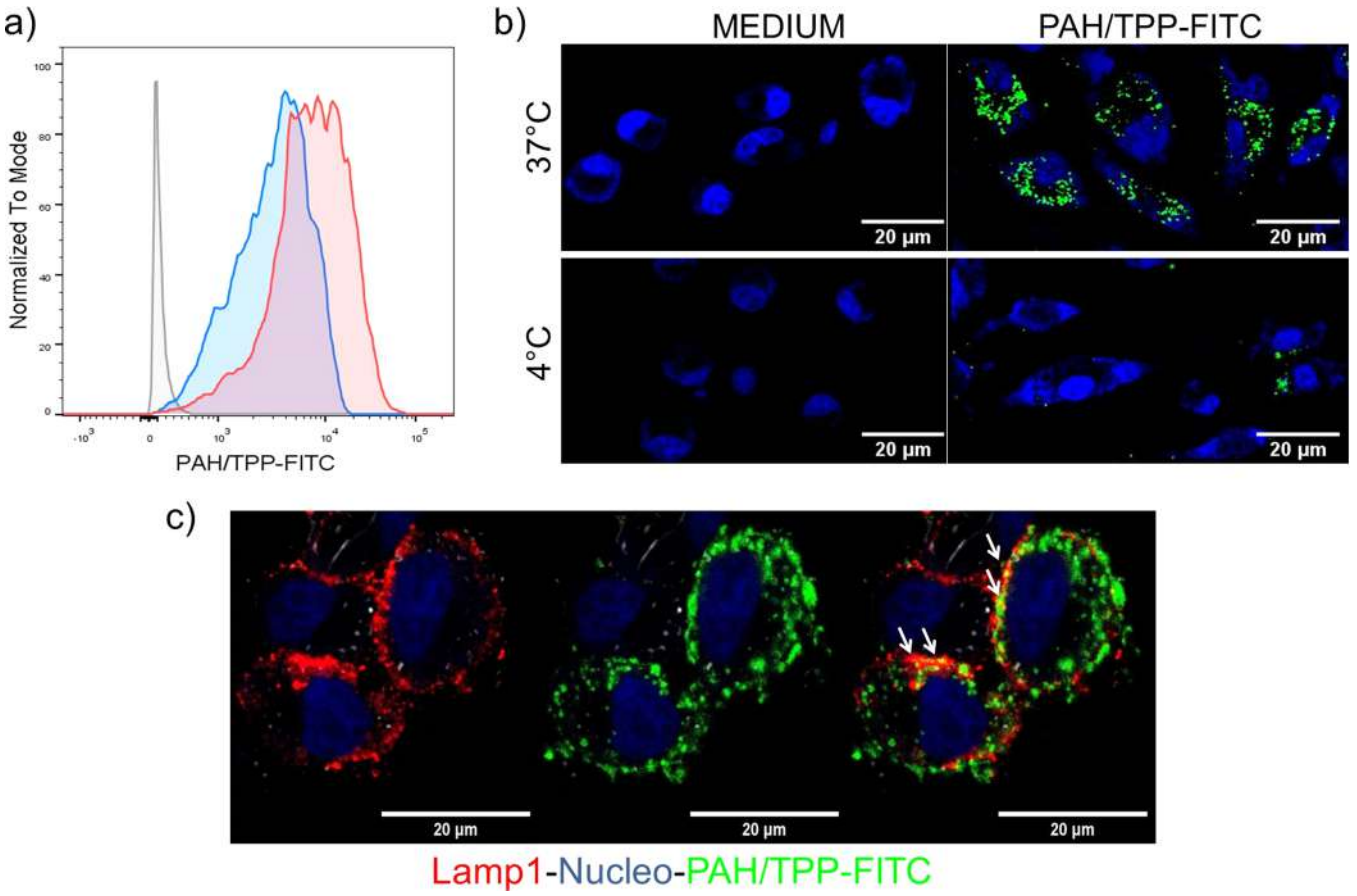

Figure 6. PAH-FITC/TPP nanocomplexes internalized by endocytosis by BMDM and analyzed by confocal microscopy and flow cytometry. (a, b) Inhibition of endocytosis performing the stimulation at 4 °C (lower panel and blue histogram) and at 37 °C (upper panel and red histogram) and (c) colocalization (yellow dots) of PAH-FITC/TPP nanocomplexes (green) in lysosomes (LAMP1 red) indicated with white arrows.

act with nanoparticulate platforms is relevant for potential immune therapy strategies mediated by antigen nanodelivery.

In this work, we focus on the interaction between PAH/TPP nanocomplexes and professional antigen-presenting cells (APCs) using bone-marrow-derived macrophages (BMDMs). BMDMs were stimulated with PAH-FITC/TPP nanocomplexes and selected by flow cytometry with the characteristic surface markers MHCII and F4/80 (see Figure S11). Figure 6a shows the fluorescence of cells exposed to PAH-FITC/TPP nanocomplexes (red histogram). On the other hand, when endocytosis is inhibited at 4 °C, cells show less fluorescence. We found that macrophages rapidly engulfed PAH-FITC/TPP nanocomplexes as cells incubated at 37 °C for 4 h showed fluorescent vesicles compared with cells stimulated at 4 °C (Figure 6b). A necessary condition for internalization is the firm adhesion of the nanocomplex onto the cell surface, which is mediated by attributes such as size, shape, and surface properties[40] It is widely recognized that positively charged nanosystems tend to have a higher cellular uptake than negatively charged ones due to the electrostatic interaction they establish with negatively charged cell membranes.[75] However, for the same reason, cationic nanocarriers may be highly toxic. In contrast, anionic nanosystems are safer but tend to have a poor cell penetration rate.[76] Interestingly, our nontoxic anionic nanocomplexes showed an efficient cellular uptake in macrophages. This may be due to the interaction between the negatively charged phosphate groups in the cell membranes and the free amine groups in the PAH/TPP nanocomplexes.

To further investigate if PAH-FITC/TPP nanocomplexes localized in the vesicles, we costained the cells with the LAMP-1 marker for lysosomes. Figure 6c shows that most of the fluorescence was located in the lysosomes, whereas some staining was observed in the cytosol and in LAMP-1 negative lysosomes; maybe they could be early endosomes. Currently, uptake into lysosomes has received more attention because nanocomplexes or nanoparticles reaching lysosomes can induce mechanical or chemical lysosomal rupture.[77] This process has also been useful for optimizing vaccine efficiency and drug delivery even for cancer treatments.[78]

CONCLUSIONS

In this work, we conducted a comprehensive study of the PAH/TPP system as a coacervate-like nanocarrier from both physicochemical and biological perspectives. In summary, our results demonstrate that by carefully adjusting the preparation parameters, it is possible to obtain PAH/TPP nanocomplexes that exhibit remarkable colloidal stability in pure water (maintaining stability for 9 months) and in cell culture media. Furthermore, these systems have the capability to efficiently encapsulate various proteins with loading efficiencies ranging from 15 to 20%. *In vitro* studies conducted in cellular media also indicate that the nanocomplexes do not induce significant cytotoxicity, hemotoxicity, or genotoxicity, unlike free PAH. Additionally, cellular internalization studies reveal

https://doi.org/10.1021/acsabm.3c00489
ACS Appl. Bio Mater. 2023, 6, 4714−4727

that the nanocomplexes are effectively internalized by macrophage cells through endocytosis and are preferentially located in lysosomes.

Overall, the results of this study address the primary question posed in the title, suggesting that nanocomplexes fabricated using a simple, fast, and entirely aqueous process serve as "friendly" carriers with excellent colloidal stability and low toxicity. Our findings provide comprehensive insights into the less-explored characteristics of PAH/TPP nanocomplexes, including their colloidal stability, cellular toxicity, and internalization in immune system cells. This represents a significant and holistic advancement in the field of polyelectrolyte nanocarriers based on the ionic assembly of polyamine. Consequently, this robust and safe nanosystem holds potential for application in protein-based therapies, particularly those involving immune system targeting and activation. Lastly, our results pave the way for further biological investigations to explore the potential of these nanocomplexes in macrophage cell activation and their potential as adjuvant agents in the development of vaccine platforms.

■ ASSOCIATED CONTENT

Supporting Information

The Supporting Information is available free of charge at https://pubs.acs.org/doi/10.1021/acsabm.3c00489.

DLS parameters (size and polydispersity index) of PAH/TPP nanocomplexes as a function TPP/NH_2; PAH degree of cross-linking as a function of the TPP content; effect of pH^0 over the hydrodynamic diameter; mean hydrodynamic diameter depending on the preparation method of the complexes; hydrodynamic diameter, polydispersity index, and histogram of sizes of 10 samples of PAH/TPP nanocomplexes prepared independently using the same protocol; long-term evolution of the hydrodynamic diameter and the derived count rate of the nanocomplexes; AFM imaging of PAH/TPP nanocomplexes; evolution of hydrodynamic diameter and polydispersity index (PDI) as a function of time; A549 cell viability in the presence of PAH; aspect of sheep RBC suspension after incubation with PAH−TPP or free PAH; and selection by flow cytometry of BMDM MHC II and F4/80 positive cells after stimulation with nanocomplexes (PDF)

■ AUTHOR INFORMATION

Corresponding Authors

Maximiliano Agazzi − *Instituto para el Desarrollo Agroindustrial y de la Salud (IDAS), (UNRC, CONICET), 5800 Río Cuarto, Córdoba, Argentina;* orcid.org/0000-0002-3065-8554; Email: magazzi@exa.unrc.edu.ar

Santiago E. Herrera − *Instituto de Química de los Materiales, Ambiente y Energía (INQUIMAE), (UBA, CONICET), C1428EGA Buenos Aires, Argentina;* orcid.org/0000-0002-8327-3914; Email: sherrera@qi.fcen.uba.ar

Omar Azzaroni − *Instituto de Investigaciones Fisicoquímicas Teóricas y Aplicadas (INIFTA), (UNLP, CONICET), 1900 La Plata, Buenos Aires, Argentina;* orcid.org/0000-0002-5098-0612; Email: omarazzaroni@quimica.unlp.edu.ar

Authors

Eugenia Apuzzo − *Instituto de Investigaciones Fisicoquímicas Teóricas y Aplicadas (INIFTA), (UNLP, CONICET), 1900 La Plata, Buenos Aires, Argentina*

Agustín Picco − *Instituto de Investigaciones Fisicoquímicas Teóricas y Aplicadas (INIFTA), (UNLP, CONICET), 1900 La Plata, Buenos Aires, Argentina*

Gastón Rizzo − *Instituto de Estudios Inmunológicos y Fisiopatológicos (IIFP), (UNLP, CONICET), asociado a CIC-PBA, 1900 La Plata, Buenos Aires, Argentina*

Camila Chavero − *Instituto de Estudios Inmunológicos y Fisiopatológicos (IIFP), (UNLP, CONICET), asociado a CIC-PBA, 1900 La Plata, Buenos Aires, Argentina*

Daiana Bianchi − *Instituto de Estudios Inmunológicos y Fisiopatológicos (IIFP), (UNLP, CONICET), asociado a CIC-PBA, 1900 La Plata, Buenos Aires, Argentina*

Paola Smaldini − *Instituto de Estudios Inmunológicos y Fisiopatológicos (IIFP), (UNLP, CONICET), asociado a CIC-PBA, 1900 La Plata, Buenos Aires, Argentina*

María Lorena Cortez − *Instituto de Investigaciones Fisicoquímicas Teóricas y Aplicadas (INIFTA), (UNLP, CONICET), 1900 La Plata, Buenos Aires, Argentina*

Waldemar A. Marmisollé − *Instituto de Investigaciones Fisicoquímicas Teóricas y Aplicadas (INIFTA), (UNLP, CONICET), 1900 La Plata, Buenos Aires, Argentina;* orcid.org/0000-0003-0031-5371

Gisel Padula − *Instituto de Genética Veterinaria "Ing. Fernando Noel Dulout" (IGEVET), (UNLP, CONICET), 1900 La Plata, Buenos Aires, Argentina; Facultad de Ciencias Naturales y Museo (FCNyM), (UNLP, CONICET), 1900 La Plata, Buenos Aires, Argentina*

Analía Seoane − *Instituto de Genética Veterinaria "Ing. Fernando Noel Dulout" (IGEVET), (UNLP, CONICET), 1900 La Plata, Buenos Aires, Argentina*

Maria Lis Alomar − *Instituto Tecnológico de Chascomús (INTECH), (UNSAM, CONICET), 7130 Chascomús, Buenos Aires, Argentina*

Maria Paula Denofrio − *Instituto Tecnológico de Chascomús (INTECH), (UNSAM, CONICET), 7130 Chascomús, Buenos Aires, Argentina*

Guillermo Docena − *Instituto de Estudios Inmunológicos y Fisiopatológicos (IIFP), (UNLP, CONICET), asociado a CIC-PBA, 1900 La Plata, Buenos Aires, Argentina*

Complete contact information is available at: https://pubs.acs.org/10.1021/acsabm.3c00489

Author Contributions

Eugenia Apuzzo: Investigation; Maximiliano Agazzi: Conceptualization, Methodology, Investigation, Supervision, Writing - original draft, Writing - review and editing; Santiago E. Herrera: Conceptualization, Methodology, Investigation, Supervision, Visualization, Writing - original draft, Writing - review and editing; Agustín S. Picco: Conceptualization, Methodology, Investigation, Supervision, Visualization, Writing - original draft, Writing - review and editing; Gastón Rizzo: Investigation, Writing - original draft; Camila Chavero: Investigation; Daiana Bianchi: Investigation; Paola Smaldini: Investigation; Lorena Cortez: Conceptualization, Writing - review and editing; Waldemar Marmisollé: Conceptualization, Writing - review and editing, Resources; Gisel Padula: Investigation; Analía Seoane: Supervision, Resources; Maria Lis Alomar: Investigation; M. Paula Denofrio: Investigation; Resources; Guillermo Docena: Supervision, Writing - review

https://doi.org/10.1021/acsabm.3c00489
ACS Appl. Bio Mater. 2023, 6, 4714−4727

and editing, Resources; Omar Azzaroni: Conceptualization, Supervision, Writing - review and editing, Resources.

Notes

The authors declare no competing financial interest.

■ ACKNOWLEDGMENTS

E.A., C.C. and G.R. are fellows of CONICET; D.B. is fellow of UNLP; M.A., S.E.H., A.S.P., P.S., L.C., W.M., G.P., A.S., M.A., M.P.D., G.H.D., and O.A. are researchers of CONICET. W.A.M. and O.A. acknowledge the financial support from Universidad Nacional de La Plata (PPID-X867), CONICET (PIP-0370), and ANPCyT (PICT-2017-1523, PICT2018-00780, and PICT2016-1680). G.H.D. acknowledges the financial support from ANPCyT (PICT 2018-2479, PICT 2020-3166) and UNLP (grant 11/X695). S.E.H. acknowledges the financial support from ANPCyT (PICT 2020-0035, PICT 2020-1758)

■ REFERENCES

(1) Cao, D.; Chen, L.; Zhang, Z.; Luo, Y.; Zhao, L.; Yuan, C.; Lu, J.; Liu, X.; Li, J. Biodegradable Nanomaterials for Diagnosis and Therapy of Tumors. *J. Mater. Chem. B* **2023**, *11* (9), 1829−1848.

(2) Deiss-Yehiely, E.; Cárcamo-Oyarce, G.; Berger, A. G.; Ribbeck, K.; Hammond, P. T. PH-Responsive, Charge-Reversing Layer-by-Layer Nanoparticle Surfaces Enhance Biofilm Penetration and Eradication. *ACS Biomater. Sci. Eng.* **2023**, *9*, 4794.

(3) Boraschi, D.; Italiani, P.; Palomba, R.; Decuzzi, P.; Duschl, A.; Fadeel, B.; Moghimi, S. M. Nanoparticles and Innate Immunity: New Perspectives on Host Defence. *Semin. Immunol.* **2017**, *34*, 33−51.

(4) Luo, Y.-H.; Chang, L. W.; Lin, P. Metal-Based Nanoparticles and the Immune System: Activation, Inflammation, and Potential Applications. *Biomed Res. Int.* **2015**, *2015*, 1−12.

(5) Liu, Y.; Hardie, J.; Zhang, X.; Rotello, V. M. Effects of Engineered Nanoparticles on the Innate Immune System. *Semin. Immunol.* **2017**, *34*, 25−32.

(6) Park, J.; Champion, J. A. Effect of Antigen Structure in Subunit Vaccine Nanoparticles on Humoral Immune Responses. *ACS Biomater. Sci. Eng.* **2023**, *9* (3), 1296−1306.

(7) Gu, W.; Meng, F.; Haag, R.; Zhong, Z. Actively Targeted Nanomedicines for Precision Cancer Therapy: Concept, Construction, Challenges and Clinical Translation. *J. Controlled Release* **2021**, *329*, 676−695.

(8) Zahid, A. A.; Chakraborty, A.; Luo, W.; Coyle, A.; Paul, A. Tailoring the Inherent Properties of Biobased Nanoparticles for Nanomedicine. *ACS Biomater. Sci. Eng.* **2023**, *9*, 3972.

(9) Zhao, L.; Skwarczynski, M.; Toth, I. Polyelectrolyte-Based Platforms for the Delivery of Peptides and Proteins. *ACS Biomater. Sci. Eng.* **2019**, *5* (10), 4937−4950.

(10) Herrera, S.; Agazzi, M. L.; Apuzzo, E.; Cortez, M. L.; Marmisollé, W.; Tagliazucchi, M.; Azzaroni, O. Polyelectrolyte-Multivalent Molecule Complexes: Physicochemical Properties and Applications. *Soft Matter* **2023**, *19*, 2013.

(11) Marras, A. E.; Ting, J. M.; Stevens, K. C.; Tirrell, M. V. Advances in the Structural Design of Polyelectrolyte Complex Micelles. *J. Phys. Chem. B* **2021**, *125* (26), 7076−7089.

(12) De, R.; Song, Y. H.; Mahata, M. K.; Lee, K. T. PH-Responsive Polyelectrolyte Complexation on Upconversion Nanoparticles: A Multifunctional Nanocarrier for Protection, Delivery, and 3D-Imaging of Therapeutic Protein. *J. Mater. Chem. B* **2022**, *10* (18), 3420−3433.

(13) Coria-Oriundo, L. L.; Debais, G.; Apuzzo, E.; Herrera, S. E.; Ceolín, M.; Azzaroni, O.; Battaglini, F.; Tagliazucchi, M. Phase Behavior and Electrochemical Properties of Highly Asymmetric Redox Coacervates. *J. Phys. Chem. B* **2023**, *127* (35), 7636−7647.

(14) Lawrence, P. G.; Lapitsky, Y. Ionically Cross-Linked Poly(Allylamine) as a Stimulus-Responsive Underwater Adhesive: Ionic Strength and PH Effects. *Langmuir* **2015**, *31* (4), 1564−1574.

(15) Lapitsky, Y. Ionically Crosslinked Polyelectrolyte Nanocarriers: Recent Advances and Open Problems. *Curr. Opin. Colloid Interface Sci.* **2014**, *19* (2), 122−130.

(16) Bugnicourt, L.; Ladavière, C. Interests of Chitosan Nanoparticles Ionically Cross-Linked with Tripolyphosphate for Biomedical Applications. *Prog. Polym. Sci.* **2016**, *60*, 1−17.

(17) Chen, S.; Wang, Z.-G. Driving Force and Pathway in Polyelectrolyte Complex Coacervation. *Proc. Natl. Acad. Sci. U. S. A.* **2022**, *119* (36), e2209975119 DOI: 10.1073/pnas.2209975119.

(18) Jonassen, H.; Kjøniksen, A.-L.; Hiorth, M. Stability of Chitosan Nanoparticles Cross-Linked with Tripolyphosphate. *Biomacromolecules* **2012**, *13* (11), 3747−3756.

(19) Echeverri-Cuartas, C. E.; Gartner, C.; Lapitsky, Y. PEGylation and Folate Conjugation Effects on the Stability of Chitosan-Tripolyphosphate Nanoparticles. *Int. J. Biol. Macromol.* **2020**, *158*, 1055−1065.

(20) Yadav, M.; Goswami, P.; Paritosh, K.; Kumar, M.; Pareek, N.; Vivekanand, V. Seafood Waste: A Source for Preparation of Commercially Employable Chitin/Chitosan Materials. *Bioresour. Bioprocess.* **2019**, *6* (1), 1−20.

(21) Herrera, S. E.; Agazzi, M. L.; Cortez, M. L.; Marmisollé, W. A.; Tagliazucchi, M.; Azzaroni, O. Redox-Active Polyamine-Salt Aggregates as Multistimuli-Responsive Soft Nanoparticles. *Phys. Chem. Chem. Phys.* **2020**, *22* (14), 7440−7450.

(22) Agazzi, M. L.; Herrera, S. E.; Cortez, M. L.; Marmisollé, W. A.; Azzaroni, O. Self-Assembled Peptide Dendrigraft Supraparticles with Potential Application in PH/Enzyme-Triggered Multistage Drug Release. *Colloids Surf., B* **2020**, *190*, No. 110895.

(23) Agazzi, M. L. Insulin Delivery from Glucose-Responsive, Self-Assembled, Polyamine Nanoparticles: Smart "Sense-and-Treat" Nanocarriers Made Easy. *Chem. − A Eur. J.* **2020**, *26* (11), 2456−2463.

(24) Herrera, S. E.; Agazzi, M. L.; Cortez, M. L.; Marmisollé, W. A.; Tagliazucchi, M.; Azzaroni, O. Multitasking Polyamine/Ferrioxalate Nano-Sized Assemblies: Thermo-, Photo-, and Redox-Responsive Soft Materials Made Easy. *Chem. Commun.* **2019**, *55* (97), 14653−14656.

(25) Herrera, S. E.; Agazzi, M. L.; Cortez, M. L.; Marmisollé, W. A.; Tagliazucchi, M.; Azzaroni, O. Polyamine Colloids Cross-Linked with Phosphate Ions: Towards Understanding the Solution Phase Behavior. *ChemPhysChem* **2019**, *20* (8), 1044−1053.

(26) Agazzi, M. L.; Herrera, S. E.; Cortez, M. L.; Marmisollé, W. A.; von Bilderling, C.; Pietrasanta, L. I.; Azzaroni, O. Continuous Assembly of Supramolecular Polyamine−Phosphate Networks on Surfaces: Preparation and Permeability Properties of Nanofilms. *Soft Matter* **2019**, *15* (7), 1640−1650.

(27) Herrera, S. E.; Agazzi, M. L.; Cortez, M. L.; Marmisollé, W. A.; Bilderling, C.; Azzaroni, O. Layer-by-Layer Formation of Polyamine-Salt Aggregate/Polyelectrolyte Multilayers. Loading and Controlled Release of Probe Molecules from Self-Assembled Supramolecular Networks. *Macromol. Chem. Phys.* **2019**, *220* (15), 1900094.

(28) Brunot, C.; Ponsonnet, L.; Lagneau, C.; Farge, P.; Picart, C.; Grosgogeat, B. Cytotoxicity of Polyethyleneimine (PEI), Precursor Base Layer of Polyelectrolyte Multilayer Films. *Biomaterials* **2007**, *28* (4), 632−640.

(29) Pugsley, C. E.; Isaac, R. E.; Warren, N. J.; Behra, J. S.; Cappelle, K.; Dominguez-Espinosa, R.; Cayre, O. J. Protection of Double-Stranded RNA via Complexation with Double Hydrophilic Block Copolymers: Influence of Neutral Block Length in Biologically Relevant Environments. *Biomacromolecules* **2022**, *23* (6), 2362−2373.

(30) Hong, J. W.; Park, J. H.; Huh, K. M.; Chung, H.; Kwon, I. C.; Jeong, S. Y. PEGylated Polyethylenimine for in Vivo Local Gene Delivery Based on Lipiodolized Emulsion System. *J. Controlled Release* **2004**, *99* (1), 167−176.

(31) Fenech, M. Cytokinesis-Block Micronucleus Cytome Assay. *Nat. Protoc.* **2007**, *2* (5), 1084−1104.

(32) Singh, N. P.; McCoy, M. T.; Tice, R. R.; Schneider, E. L. A Simple Technique for Quantitation of Low Levels of DNA Damage in Individual Cells. *Exp. Cell Res.* **1988**, *175* (1), 184−191.

(33) Collins, A. R. The Comet Assay for DNA Damage and Repair: Principles, Applications, and Limitations. *Mol. Biotechnol.* **2004**, *26* (3), 249−261.
(34) Weischenfeldt, J.; Porse, B. Bone Marrow-Derived Macrophages (BMM): Isolation and Applications. *Cold Spring Harb. Protoc.* **2008**, *2008* (12), pdb.prot5080 DOI: 10.1101/pdb.prot5080.
(35) Huang, Y.; Lapitsky, Y. Determining the Colloidal Behavior of Ionically Cross-Linked Polyelectrolytes with Isothermal Titration Calorimetry. *J. Phys. Chem. B* **2013**, *117* (32), 9548−9557.
(36) Lawrence, P. G.; Lapitsky, Y. Ionically Cross-Linked Poly(Allylamine) as a Stimulus-Responsive Underwater Adhesive: Ionic Strength and PH Effects. *Langmuir* **2015**, *31* (4), 1564−1574.
(37) Zhang, Y.; Yildirim, E.; Antila, H. S.; Valenzuela, L. D.; Sammalkorpi, M.; Lutkenhaus, J. L. The Influence of Ionic Strength and Mixing Ratio on the Colloidal Stability of PDAC/PSS Polyelectrolyte Complexes. *Soft Matter* **2015**, *11* (37), 7392−7401.
(38) Laucirica, G.; Marmisollé, W. A.; Azzaroni, O. Dangerous Liaisons: Anion-Induced Protonation in Phosphate−Polyamine Interactions and Their Implications for the Charge States of Biologically Relevant Surfaces. *Phys. Chem. Chem. Phys.* **2017**, *19* (12), 8612−8620.
(39) Yuan, Y.; Huang, Y. Ionically Crosslinked Polyelectrolyte Nanoparticle Formation Mechanisms: The Significance of Mixing. *Soft Matter* **2019**, *15* (48), 9871−9880.
(40) Smokers, I. B. A.; van Haren, M. H. I.; Lu, T.; Spruijt, E. Complex Coacervation and Compartmentalized Conversion of Prebiotically Relevant Metabolites. *ChemSystemsChem.* **2022**, *4* (4), No. e202200004.
(41) Huang, Y.; Lapitsky, Y. Salt-Assisted Mechanistic Analysis of Chitosan/Tripolyphosphate Micro- and Nanogel Formation. *Biomacromolecules* **2012**, *13* (11), 3868−3876.
(42) Lawrence, P. G.; Patil, P. S.; Leipzig, N. D.; Lapitsky, Y. Ionically Cross-Linked Polymer Networks for the Multiple-Month Release of Small Molecules. *ACS Appl. Mater. Interfaces* **2016**, *8* (7), 4323−4335.
(43) Huang, Y.; Lawrence, P. G.; Lapitsky, Y. Self-Assembly of Stiff, Adhesive and Self-Healing Gels from Common Polyelectrolytes. *Langmuir* **2014**, *30* (26), 7771−7777.
(44) Yewdall, N. A.; André, A. A. M.; Lu, T.; Spruijt, E. Coacervates as Models of Membraneless Organelles. *Curr. Opin. Colloid Interface Sci.* **2021**, *52*, No. 101416.
(45) Alam, S. S.; Mather, C. B.; Seo, Y.; Lapitsky, Y. Poly(Allylamine)/Tripolyphosphate Coacervates for Encapsulation and Long-Term Release of Cetylpyridinium Chloride. *Colloids Surf., A* **2021**, *629*, No. 127490.
(46) Chen, M.-C.; Mi, F.-L.; Liao, Z.-X.; Hsiao, C.-W.; Sonaje, K.; Chung, M.-F.; Hsu, L.-W.; Sung, H.-W. Recent Advances in Chitosan-Based Nanoparticles for Oral Delivery of Macromolecules. *Adv. Drug Delivery Rev.* **2013**, *65* (6), 865−879.
(47) Mazancová, P.; Némethová, V.; Trelová, D.; Kleščíková, L.; Lacík, I.; Rázga, F. Dissociation of Chitosan/Tripolyphosphate Complexes into Separate Components upon PH Elevation. *Carbohydr. Polym.* **2018**, *192*, 104−110.
(48) Hassan, Y. I.; Lahaye, L.; Gong, M. M.; Peng, J.; Gong, J.; Liu, S.; Gay, C. G.; Yang, C. Innovative Drugs, Chemicals, and Enzymes within the Animal Production Chain. *Vet. Res.* **2018**, *49* (1), 71.
(49) Cai, Y.; Lapitsky, Y. Biomolecular Uptake Effects on Chitosan/Tripolyphosphate Micro- and Nanoparticle Stability. *Colloids Surfaces B Biointerfaces* **2020**, *193*, No. 111081.
(50) Furlani, F.; Parisse, P.; Sacco, P. On the Formation and Stability of Chitosan/Hyaluronan-Based Complex Coacervates. *Molecules* **2020**, *25* (5), 1071.
(51) Sproncken, C. C. M.; Gumí-Audenis, B.; Foroutanparsa, S.; Magana, J. R.; Voets, I. K. Controlling the Formation of Polyelectrolyte Complex Nanoparticles Using Programmable PH Reactions. *Macromolecules* **2023**, *56* (1), 226−233.
(52) Ramos, R.; Bernard, J.; Ganachaud, F.; Miserez, A. Protein-Based Encapsulation Strategies: Toward Micro- and Nanoscale Carriers with Increased Functionality. *Small Sci.* **2022**, *2* (3), 2100095.
(53) Blocher McTigue, W. C.; Perry, S. L. Incorporation of Proteins into Complex Coacervates. In *Methods in Enzymology*; 2021; pp 277−306.
(54) Blocher McTigue, W. C.; Perry, S. L. Protein Encapsulation Using Complex Coacervates: What Nature Has to Teach Us. *Small* **2020**, *16* (27), 1907671.
(55) Blocher McTigue, W. C.; Perry, S. L. Design Rules for Encapsulating Proteins into Complex Coacervates. *Soft Matter* **2019**, *15* (15), 3089−3103.
(56) Agazzi, M. L.; Paletti Rovey, M. F.; Apuzzo, E.; Herrera, S. E.; Spesia, M. B.; Oliva, M. d. las M.; Azzaroni, O. Lysozyme/Tripolyphosphate Complex Coacervates: Properties, Curcumin Encapsulation and Antibacterial Activity. *Food Hydrocoll.* **2023**, *145*, No. 109134.
(57) Ball, V.; Winterhalter, M.; Schwinte, P.; Lavalle, P.; Voegel, J.-C.; Schaaf, P. Complexation Mechanism of Bovine Serum Albumin and Poly(Allylamine Hydrochloride). *J. Phys. Chem. B* **2002**, *106* (9), 2357−2364.
(58) Lei, H.; Alu, A.; Yang, J.; He, C.; Hong, W.; Cheng, Z.; Yang, L.; Li, J.; Wang, Z.; Wang, W.; Lu, G.; Wei, X. Cationic Nanocarriers as Potent Adjuvants for Recombinant S-RBD Vaccine of SARS-CoV-2. *Signal Transduction Targeted Ther.* **2020**, *5* (1), 291.
(59) Huang, X.; Shen, S.; Zhang, Z.; Zhuang, J. Cross-Linked Polyethylenimine-Tripolyphosphate Nanoparticles for Gene Delivery. *Int. J. Nanomedicine* **2014**, *4785*, 4785.
(60) Wada, T.; Kano, A.; Shimada, N.; Maruyama, A. α-Amino Acid Pendant Polymers as Endosomal PH-Responsive Gene Carriers. *Macromol. Res.* **2012**, *20* (3), 302−308.
(61) Di Silvio, D.; Martínez-Moro, M.; Salvador, C.; de los Angeles Ramirez, M.; Caceres-Velez, P. R.; Ortore, M. G.; Dupin, D.; Andreozzi, P.; Moya, S. E. Self-Assembly of Poly(Allylamine)/SiRNA Nanoparticles, Their Intracellular Fate and SiRNA Delivery. *J. Colloid Interface Sci.* **2019**, *557*, 757−766.
(62) Venault, A.; Huang, Y.-C.; Lo, J. W.; Chou, C.-J.; Chinnathambi, A.; Higuchi, A.; Chen, W.-S.; Chen, W.-Y.; Chang, Y. Tunable PEGylation of Branch-Type PEI/DNA Polyplexes with a Compromise of Low Cytotoxicity and High Transgene Expression: In Vitro and in Vivo Gene Delivery. *J. Mater. Chem. B* **2017**, *5* (24), 4732−4744.
(63) Andreozzi, P.; Simó, C.; Moretti, P.; Porcel, J. M.; Lüdtke, T. U.; Ramirez, M. de los A.; Tamberi, L.; Marradi, M.; Amenitsch, H.; Llop, J.; Ortore, M. G.; Moya, S. E. Novel Core−Shell Polyamine Phosphate Nanoparticles Self-Assembled from PEGylated Poly(Allylamine Hydrochloride) with Low Toxicity and Increased In Vivo Circulation Time. *Small* **2021**, *17* (35), 2102211.
(64) Kodama, Y.; Kuramoto, H.; Mieda, Y.; Muro, T.; Nakagawa, H.; Kurosaki, T.; Sakaguchi, M.; Nakamura, T.; Kitahara, T.; Sasaki, H. Application of Biodegradable Dendrigraft Poly-l-Lysine to a Small Interfering RNA Delivery System. *J. Drug Target.* **2017**, *25* (1), 49−57.
(65) Qiu, T. A.; Torelli, M. D.; Vartanian, A. M.; Rackstraw, N. B.; Buchman, J. T.; Jacob, L. M.; Murphy, C. J.; Hamers, R. J.; Haynes, C. L. Quantification of Free Polyelectrolytes Present in Colloidal Suspension, Revealing a Source of Toxic Responses for Polyelectrolyte-Wrapped Gold Nanoparticles. *Anal. Chem.* **2017**, *89* (3), 1823−1830.
(66) Mosmann, T. Rapid Colorimetric Assay for Cellular Growth and Survival: Application to Proliferation and Cytotoxicity Assays. *J. Immunol. Methods* **1983**, *65* (1−2), 55−63.
(67) Boussif, O.; Delair, T.; Brua, C.; Veron, L.; Pavirani, A.; Kolbe, H. V. J. Synthesis of Polyallylamine Derivatives and Their Use as Gene Transfer Vectors in Vitro. *Bioconjugate Chem.* **1999**, *10* (5), 877−883.
(68) Matsuzawa, T.; Ikarashi, Y. Haemolysis of Various Mammalian Erythrocytes in Sodium Chloride, Glucose and Phosphate-Buffer Solutions. *Lab. Anim.* **1979**, *13* (4), 329−331.

(69) Goodhead, L. K.; MacMillan, F. M. Measuring Osmosis and Hemolysis of Red Blood Cells. *Adv. Physiol. Educ.* **2017**, *41* (2), 298−305.
(70) Alameh, M.; Lavertu, M.; Tran-Khanh, N.; Chang, C.-Y.; Lesage, F.; Bail, M.; Darras, V.; Chevrier, A.; Buschmann, M. D. SiRNA Delivery with Chitosan: Influence of Chitosan Molecular Weight, Degree of Deacetylation, and Amine to Phosphate Ratio on in Vitro Silencing Efficiency, Hemocompatibility, Biodistribution, and in Vivo Efficacy. *Biomacromolecules* **2018**, *19* (1), 112−131.
(71) Chen, L.; Simpson, J. D.; Fuchs, A. V.; Rolfe, B. E.; Thurecht, K. J. Effects of Surface Charge of Hyperbranched Polymers on Cytotoxicity, Dynamic Cellular Uptake and Localization, Hemotoxicity, and Pharmacokinetics in Mice. *Mol. Pharmaceutics* **2017**, *14* (12), 4485−4497.
(72) Kumari, A.; Kumari, K.; Gupta, S. Protease Responsive Essential Amino-Acid Based Nanocarriers for Near-Infrared Imaging. *Sci. Rep.* **2019**, *9* (1), 20334.
(73) Jo, E.-K.; Kim, J. K.; Shin, D.-M.; Sasakawa, C. Molecular Mechanisms Regulating NLRP3 Inflammasome Activation. *Cell. Mol. Immunol.* **2016**, *13* (2), 148−159.
(74) Moser, M.; Leo, O. Key Concepts in Immunology. *Vaccine* **2010**, *28*, C2−C13.
(75) Sanità, G.; Carrese, B.; Lamberti, A. Nanoparticle Surface Functionalization: How to Improve Biocompatibility and Cellular Internalization. *Front. Mol. Biosci.* **2020**, *7*, No. 587012.
(76) Genito, C. J.; Batty, C. J.; Bachelder, E. M.; Ainslie, K. M. Considerations for Size, Surface Charge, Polymer Degradation, Co-Delivery, and Manufacturability in the Development of Polymeric Particle Vaccines for Infectious Diseases. *Adv. NanoBiomed Res.* **2021**, *1* (3), 2000041.
(77) Serrano-Puebla, A.; Boya, P. Lysosomal Membrane Permeabilization in Cell Death: New Evidence and Implications for Health and Disease. *Ann. N. Y. Acad. Sci.* **2016**, *1371* (1), 30−44.
(78) Wang, C.; Li, P.; Liu, L.; Pan, H.; Li, H.; Cai, L.; Ma, Y. Self-Adjuvanted Nanovaccine for Cancer Immunotherapy: Role of Lysosomal Rupture-Induced ROS in MHC Class I Antigen Presentation. *Biomaterials* **2016**, *79*, 88−100.

https://doi.org/10.1021/acsabm.3c00489
ACS Appl. Bio Mater. 2023, 6, 4714−4727